Constraint Inversion Algorithm of Lidar Equation for Deriving Aerosol Optical Property①

Qiu Jinhuan (邱金桓)

Institute of Atmospheric Physics, Chinese Academy of Sciences, Beijing 100080

(Received April 21, 1998)

ABSTRACT

A key question of the backward integration algorithm to lidar equation is how to determine the far-end boundary value. This paper develops a Constraint Inversion Algorithm (CIA) for deriving the value and then the aerosol extinction profile from lidar signals, which uses the ground-level horizontal lidar signals as the constraint information. The smaller the wavelength is, the more sensitive to the variation of aerosol extinction to backscatter ratio solved by CIA. According to the property an algorithm is further proposed to simultaneously retrieve the aerosol extinction profile, the size distribution and the imaginary part of its reflective index from the multi-wavelength lidar observations. CIA is tested in the inversion simulations with satisfactory result.

Key words: Constraint inversion, Boundary value, Aerosol optical property

1. Introduction

Lidar is increasingly used in measuring the optical properties of aerosols and clouds since the 1960's. It has been shown that the determination of the extinction coefficient as a function of height is feasible (Klett, 1980; Fernald, 1984; Lu Daren et al., 1977; Spinhirne et al., 1983). However, some theoretical difficulties in deriving quantitatively the extinction profile in the tropospheric atmosphere have not yet been solved.

A strong sensitivity of the lidar equation solution to a near-end boundary value in the case of a turbid atmosphere by using Forward Integration Algorithm has been analyzed by Klett (1980). Klett's Backward Integration Algorithm can be more stable, but it is confronted with a difficulty how to determine the far-end boundary value. Therefore, many authors have paid much attention on studies of inversion algorithms, including the question of selecting a boundary value (Ferguson and Stephens, 1983; Qiu, 1988), two-wavelength algorithm (Potter, 1987; Qiu 1995), and the solution stability of the lidar equation with two components (Sasano and Nakene,1984). Most methods for determining the boundary value are based on the assumption of homogeneity near the far-end.

The assumption of the optically homogeneous atmosphere cannot usually be suitable in the case of vertical or slant lidar observation. In addition, the aerosol size distribution and its reflective index are very important for the studies of the aerosol radiation-climate effect, the atmospheric correction of spaceborne remote sensing and so on. But up to now, there has been a limited study on lidar measurement of the distribution and the reflective index. This paper develops a Constraint Inversion Algorithm (CIA) for determining the far-end boundary value (aerosol extinction coefficient) and then the aerosol extinction profile from the

①This research was supported by the National Natural Science Foundation of China.

vertical or slant lidar signals without an assumption of the homogeneous atmosphere near the far-end. The algorithm uses the ground-level horizontal signals as the constraint information for the determination. As shown in next inversion simulations, the smaller the wavelength is, the more sensitive to the variation of the aerosol extinction to backscatter ratio solved by CIA. Based on the property, the constraint inversion algorithm using the multi-wavelength lidar signals is further proposed to simultaneously retrieve the aerosol extinction profile, the extinction to backscatter ratio, the size distribution and the imaginary part of its reflective index.

2. CIA for deriving aerosol extinction coefficiet profile

The lidar equation can be written as

$$P(r)=\frac{CE[\beta_m(r)+\beta_a(r)]}{r^2}e^{-2\int_0^r[\sigma_m(r)+\sigma_a(r)]dr}, \tag{1}$$

where $P(r)$ is the lidar return signal from the atmosphere at the distance r, C is a constant of lidar system, E is the laser output energy, $\beta_m(r)$ and $\sigma_m(r)$ are respectively the molecular backscatter coefficient and the extinction coefficient, and $\beta_a(r)$ and $\sigma_a(r)$ are the aerosol backscatter and extinction coefficients, respectively.

Derived from Eq.1, the aerosol extinction coefficient solved by the backward integration algorithm is:

$$\sigma_a(r)=-\alpha(r)\sigma_m(r)+\frac{S(r)\exp[2(\alpha(r)-1)\int_r^{r_1}\sigma_m(r)dr]}{S(r_1)/[\sigma_a(r_1)+\alpha(r_1)\sigma_m(r_1)]+2\int_r^{r_1}S(r)\exp\left\{2[\alpha(r)-1]\int_r^{r_1}\sigma_m(r'')dr''\right\}dr}, \tag{2}$$

where $\alpha(r)=k_a(r)/k_m$, $k_a(r)$ and k_m are the aerosol and molecular extinction to backscatter ratios, respectively, $S(r)=P(r)r^2$, and $\sigma_a(r_1)$ is the so-called far-end boundary value to be determined, i.e. the aerosol extinction coefficient at the far-end distance r_1. Under the condition of known molecular parameters and $k_a(r)$, the solution $\sigma_a(r)$ can be derived using Eq.2, if the boundary value $\sigma_a(r_1)$ can be determined. Next, CIA for deriving the value is proposed.

It is derived from Eq.1 that

$$\begin{aligned}\mathcal{J}(r)&=\int_{r_0}^{r}k_a(r)S(r)\exp\left\{2\int_0^r[1-\alpha(r'')]\sigma_m(r'')dr''\right\}dr\\&=\frac{CE}{2}\{\exp[-2\alpha(r_0)\tau_m(0,r_0)-2\tau_a(0,r_0)]-\exp[-2\tau_a(0,r)-2\alpha(r)\tau_m(0,r)]\},\end{aligned} \tag{3}$$

where τ_a and τ_m are the aerosol and molecular optical depths, respectively.

Combining Eqs.1-3 can yield the expression for the far-end extinction coefficient $\sigma_a(r_1)$ as:

$$\begin{aligned}\sigma_a(r_1)=&-\alpha(r_1)\sigma_m(r_1)+S(r_1)k_a(r_1)\{\exp[2\tau_m(0,r_1)+2\tau_a(r_0,r_1)\\&-2\alpha(r_0)\tau_m(0,r_0)]-\exp[2\tau_m(0,r_1)-2\alpha(r_1)\tau_m(0,r_1)]\}/\mathcal{J}(r_1).\end{aligned} \tag{4}$$

If the molecular parameters and $k_a(r)$ are known, only the optical depth $\tau_a(r_0,r_1)$ is

needed for the determination of $\sigma_a(r_1)$. The so-called Constraint Inversion Algorithm (CIA) proposed in this paper uses the additional lidar signals and $\tau_{ah}(r_0, r_{1h})$ derived from the signals along the ground-level horizontal path as constraint information in determining $\tau_a(r_0, r_1)$ along slant (or vertical) path.

Both horizontal and slant lidar return signals meet Eq.3. Adding a subscript h to the parameters in Eq.3 to represent the horizontal case, it can be derived from the horizontal lidar signals that:

$$\begin{aligned} f_h(r) &= \int_{r_0}^{r} k_{ah}(r) S_h(r) \exp\{2\int_0^r [1-\alpha_h(r'')]\sigma_{mh}(r'')dr''\}dr \\ &= \frac{CE_h}{2}\{\exp[-2\alpha_h(r_0)\tau_{mh}(0, r_0) - 2\tau_{ah}(0, r_0)] \\ &\quad - \exp[-2\tau_{ah}(0, r) - 2\alpha_h(r)\tau_{mh}(0, r)]\} \ . \end{aligned} \tag{5}$$

The same near-end distance r_0 can usually be used for the two cases of horizontal and slant paths. Then based on Eq.3 and Eq.5, $\tau_a(r_0, r_1)$ can be determined as:

$$\tau_a(r_0, r_1) = -\frac{k_a(r_1)}{k_m}\tau_m(r_0, r_1) - 0.5\ln\left[1 - \frac{GBEf(r_1)}{E_h f_h(r_{1h})}\right] , \tag{6}$$

$$G = 1 - \exp[-2\tau_{ah}(r_0, r_{1h}) - 2\alpha_h(r_{1h})\tau_{mh}(r_0, r_{1h})] , \tag{7}$$

$$B = -\exp[-2\tau_a(0, r_0) - 2\alpha(r_0)\tau_m(0, r_0) + 2\tau_{ah}(0, r_0) + 2\alpha_h(r_0)\tau_{mh}(0, r_0)] . \tag{8}$$

Here r_{1h} is the far-end distance for the horizontal path. If $k_a(r)$ is known, $f(r_1)$ and $f(r_{1h})$ can be determined. $G \approx 1 - \exp[-2\tau_{ah}(r_0, r_{1h})]$. The optical depth $\tau_{ah}(r_0, r_{1h})$ can be derived from the horizontal lidar signals and then used in determining G. In the case of small r_0 or basically homogeneous aerosol extinction coefficient between 0 and r_0, $B = 1$ is available. If r_0 is large, B can be determined through adding lidar observation with a low elevation angle, which will be studied in the future experiment. Therefore, if $k_a(r)$ is known, using the above-presented algorithm, the optical depth $\tau_a(r_0, r_1)$ and then the far-end boundary value $\sigma_a(r_1)$ along the slant path can be determined.

In the case of height-independent $k_a(r)$ and that the molecular scatter is negligible, Eqs.6–8 can be simplified as:

$$\tau_a(r_0, r_1) = -0.5\ln\left[1 - \frac{GBEf(r_1)}{E_h f_h(r_{1h})}\right] , \tag{9}$$

$$G = 1 - \exp[-2\tau_{ah}(r_0, r_{1h})] , \tag{10}$$

$$B = \exp[-2\tau_a(0, r_0) + 2\tau_{ah}(0, r_0)] , \tag{11}$$

$$f(r_1) / f_h(r_{1h}) = \int_{r_0}^{r_1} S(r)dr \Big/ \int_{r_0}^{r_{1h}} S_h(r)dr \ . \tag{12}$$

In fact, it is difficult to consider or derive height-dependent $k_a(r)$ according to the lidar return signals. In next inversion simulations, an assumption of height-independent $k_a(r)$ is made, but its effect on the solution is studied.

3. CIA for deriving aerosol extinction profiles, size distribution and reflective index from multi-wavelength lidar signals

As shown in next inversion simulations, the shorter the wavelength is, the more sensitive to the variation of k_a the extinction profile solution $\sigma_a(r)$ by CIA. According to the property an algorithm is further proposed to simultaneously retrieve $\sigma_a(r)$, k_a, aerosol size distribution and imaginary part of its reflective index from the multi-wavelength lidar observations. In the algorithm, Junge size distribution is assumed, which is given by

$$n(r) = cr^{-(1+\nu^*)} . \tag{13}$$

Next, a two-wavelength iterative algorithm for the simultaneous retrieval of $\sigma_a(r)$, k_a and ν^* is presented. The two Nd-YAG laser wavelengths of $\lambda_1 = 1060$ nm and $\lambda_2 = 532$ nm are taken as an example of wavelength selection. In the algorithm k_a is retrieved from the λ_2 lidar signals through setting the far-end extinction coefficient solution $\sigma_a(r_1)$ being equal to a given value δ. At first, $\delta = 0$ is taken, which is explained in next simulations. The iterative algorithm goes like this:

(1) Set $n = 0$ and $\delta^{(0)} = 0.0$.

(2) Selecting the different values of k_a, derive the far-end extinction coefficient $\sigma_{a,2}(r_1)$ from the λ_2 lidar signals by using CIA. The value of k_a, corresponding with $\sigma_{a,2}(r_1) = \delta^{(n)}$, is taken as its solution and marked as $k_{a,n}$, and corresponding aerosol extinction coefficient profile and its optical depth solutions are marked as $\sigma_{a,2}(r)$ and $\tau_{a,2}(r)$.

(3) Using the value $k_{a,n}$, derive the λ_1-wavelength optical depth $\tau_{a,1}$ and its extinction coefficient profile $\sigma_{a,1}(r)$ from the λ_1 lidar signals.

(4) Derive the Junge parameter ν^* using the following formula:

$$\nu^* = \log(\tau_{a,2} / \tau_{a,1}) / \log(\lambda_1 / \lambda_2) + 2 . \tag{14}$$

(5) Set

$$\delta^{(n)} = \sigma_{a,1}(r_1)(\lambda_1 / \lambda_2)^{(\nu^* - 2)} . \tag{15}$$

(6) Let $\Delta = abs(k_{a,n} - k_{a,n-1})$, and $n = n + 1$.

(7) If Δ is small enough ($\Delta < 0.05$ is taken in this paper), stop the iterative process, otherwise repeat Steps 2-7.

The final $k_{a,n}$, ν^*, $\sigma_{a,1}(r)$ and $\sigma_{a,2}(r)$ are taken as their solutions. In this algorithm the determination of k_a is based on the stronger sensitivity of the far-end extinction coefficient solution to the variation of k_a for the λ_2-wavelenth, and the retrieved λ_2-wavelenth k_a is used in deriving the λ_1-wavelenth aerosol extinction coefficient profile.

The extinction to backscatter ratio k_a is more sensitive to the variation of the imaginary part of aerosol reflective index than its real part. Under the assumption of Junge size distribution and a known real part, k_a is only dependent on the imaginary part n_i and ν^*, and thus n_i can easily be determined by using the solutions of k_a and ν^* through the Mie scattering calculation. In the present algorithm, the different imaginary parts are selected in calculating k_a, and the imaginary part n_i, corresponding with the solution of k_a, is taken as its solution.

4. Inversion simulations

a. *Input parameters*

In numerical simulations, the two Nd–YAG laser wavelengths of $\lambda = 1060$ nm and 532 nm are selected. Figure 1 shows two 0.55 μm–wavelength aerosol extinction coefficient profiles used in simulations. One is the model presented by Elterman (1964), taken as the clear model. And another is the turbid model, in which the 0.55 μm extinction coefficient from the ground to 1 km height is equal to 0.5, above 2 km it is the same as that in the Elterman's model, and between 1 km and 2 km it is linearly interpolated. The 1060 nm and 532 nm extinction profiles are derived from the 0.55 μm profiles according to the power–law or Mie scattering calculation.

One aerosol size distribution used is the Junge distribution of $\nu^* = 3$. In the case, the dependence of extinction coefficient on the wavelength follows λ^{-1}–power law. And as the distribution is used, $k_a = 40$ is taken as the exact extinction to backscatter ratio.

Tables 1–2 show another two aerosol types used, i.e. continent and urban models presented by Lenoble (1985). Lenoble's continent and urban aerosol models are all composed of the three components of fine, coarse and fine soot aerosol, which have different log–normal size distributions, volume percentages and reflective index. In the column of "Volume percentage", the first set of digits are corresponding to the continent aerosol, and the second urban. As shown in Table 1, the volume percentages of the three components are 29, 70 and 1 for continent, and 61, 17 and 22 for urban. Aerosol imaginary part is very different. It is 0.008 for the fine aerosol. For the coarse, it is 0.017 and 0.006 for the 1060 nm and 532 nm wavelengths, respectively. And for the fine soot, it is 0.44 for the two wavelengths. Real part of aerosol reflective index (not listed in Table 1), is 1.53 for the first two components and 1.75 for the fine soot. The values of k_a in Table 1 are determined according to the Mie calculation and using the above–mentioned aerosol parameters. They, varying between 26 and 117.2, are much variable for different aerosol components and wavelengths. In Table 2, k_a is the extinction to backscatter ratio of aerosol mixture composed of the three components, and ν^* is the Junge size distribution fitted from the two extinction coefficients of 1060 nm and 532 nm. For the continent aerosol, k_a is 37.8 and 38.1 for the 1060 nm and 532 nm wavelengths, respectively. And for the urban aerosol, it is 55.9 and 46.6, showing a strong wavelength–dependence. ν^* is 3.029 and 3.358 for the continent and urban aerosol, respectively. Similar to Lenoble's study, height–independent k_a and ν^* are used for the continent aerosol extinction profile. And for the turbid extinction profile, k_a and ν^* are taken from the continent and urban model parameters for 0–2 km and above 2 km, respectively. So in the case of urban model, k_a is closely related to height and wavelength.

In addition, all numerical simulations select 20 m resolution and vertical observation path, and $r_0 = 200$ m. If there is no additional explanation, $r_1 = r_{1h}$ is taken.

Table 1. Aerosol construction parameters

Size distribution	Volume percentage	Imaginary part (1060 / 532 nm)	k_a (1060 / 532 nm)
Fine	29 / 61	0.008 / 0.008	46.3 / 35.1
Coarse	70 / 17	0.017 / 0.006	26.0 / 40.4
Fine soot	1 / 22	0.44 / 0.44	117.2 / 78.4

Table 2. Extinction to backscatter ratio of aerosol mixure

Wavelength (nm)	1060	532	ν^*
Continental k_a	37.8	38.1	3.029
Urban k_a	55.9	46.6	3.358

b. *Inversion results of aerosol extinction coefficient profiles*

It can be found from Eqs.2–6 that the error factors of lidar equation solution by CIA are mainly: (1) error of lidar return signals, (2) measurement error of optical depth $\tau_{ah}(r_{0h}, r_{1h})$ along referenced (horizontal) path, (3) uncertainty of k_a and, (4) error in output energy ratio, E / E_h.

If the output energy is stable and there are a lot of laser shots along every sounding path, $E / E_0 = 1$ can be taken. If there is an energy monitor, it can be used in determining the ratio E / E_0, and through a lot of laser shots good accuracy can be realized.

Next, according to the numerical simulations shown in Figs. 2–8 and Table 3, the first three error factors are analyzed. The clear aerosol extinction model, Junge size distribution with $\nu^* = 3$, and $k_a = 40$ are taken in Figs. 2–7. In Fig. 8, the turbid aerosol extinction model and corresponding k_a shown in Table 2 are used.

(1) *Effect of lidar signal error*

Based on Fig. 2 and Table 3, the effect of lidar signal error is studied. A random error sequence in lidar signal is designed as:

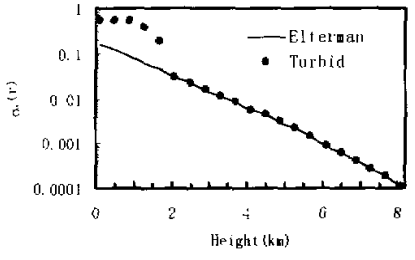

Fig. 1. Aerosol extinction coefficient profiles used in inversion simulations.

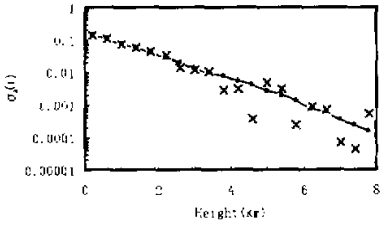

Fig. 2. True 532 nm extinction coefficient profile (solid line), solution (circles) without input parameter error and solution (crosses) with random signal error within ±10%.

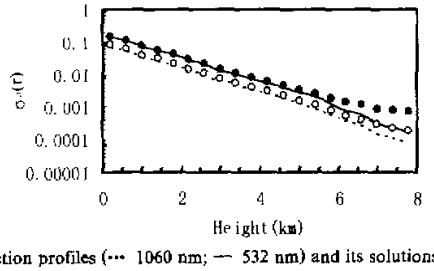

Fig. 3. True extinction profiles (··· 1060 nm; — 532 nm) and its solutions (∘ 1060 nm; • 532 nm) with an error of 10% in horizontal optical depth.

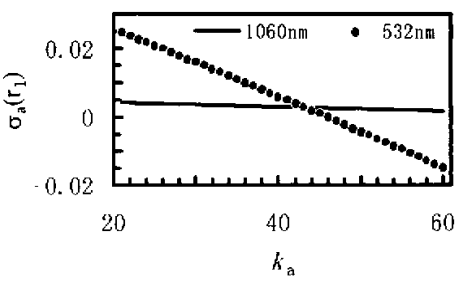

Fig. 4. Retrieved far-end extinction coefficient $\sigma_a(r_1)$ verse k_a for $r_1 = 8$ km.

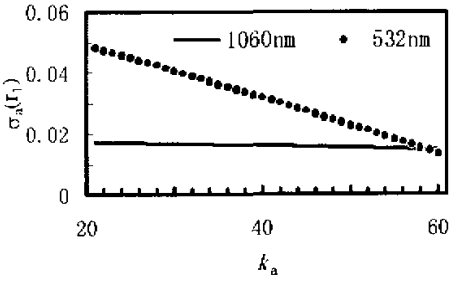

Fig. 5. Same as in Fig. 4 but for $r_1 = 2$ km.

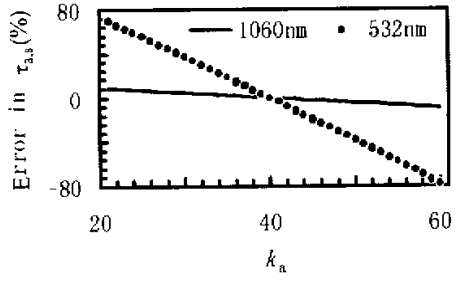

Fig. 6. Percent error of optical depth solution caused by uncertainty in k_a for $r_1 = 8$ km

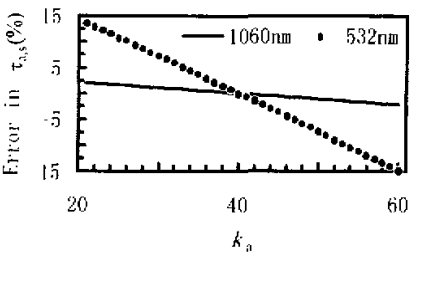

Fig. 7. Percent error of optical depth solution caused uncertainty in k_a for $r_1 = 2$ km.

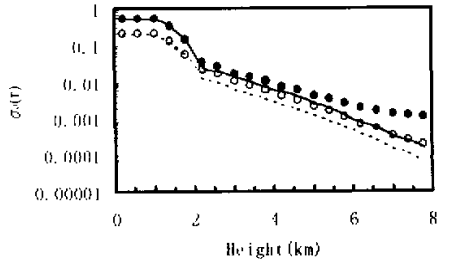

Fig. 8. True extinction profiles (··· 1060 nm; — 532 nm) and its solutions (∘ 1060 nm; • 532 nm) using the urban k_a in simulations.

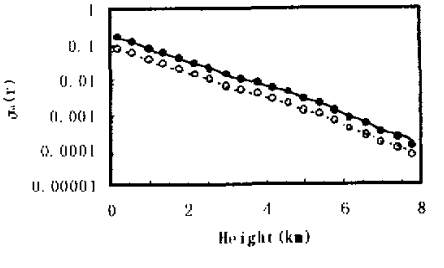

Fig. 9. True extinction profiles (··· 1060 nm; — 532 nm) and its solutions (∘ 1060 nm; • 532 nm) for clear model.

$$\delta(r_i) = 2(1 - t_i)D \ , \tag{16}$$

where t_i is ramdom number taken from computer and changing from 0 to 1. If $D = 0.1$, $\delta(r)$ and then lidar signal error would range within ± 10%.

Figure 2 shows the 0.532 nm extinction coefficient profile solutions for the clear model in the two cases of no error in all input parameters and random signal errors with $D = 0.1$ (signal errors being within ± 10%). In the case of no signal error, a very good solution is obtained. In another case with the random signal error, the solution is also satisfactory, but a

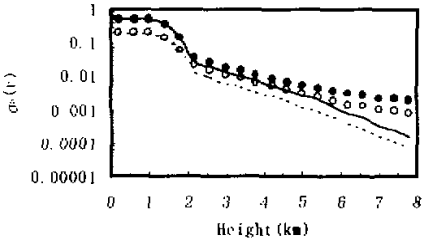

Fig. 10. Same as Fig. 10 but for turbid model.

vibration deviation of the solution to its true profile is found. Where $\delta(r) < 0$ (underestimated signal error), the retrieved extinction coefficient is underestimated, and where $\delta(r) > 0$, it is overestimated. As a result, as shown in Table 3, the error in the optical depth solution can be very small. In Table 3, $\Delta\tau_{a,1}$ and $\Delta\tau_{a,2}$ stand for the percent errors in the 1060 nm and 532 nm optical depth solutions between 0.2 km and 8 km, respectively. All optical depth solutions with $D = 0.05$, 0.1 and 0.2 have an accuracy better than 4.9%, even as the lidar signal errors are up to ± 20%. The 1060 nm solution is of smaller error. For the inversion result shown in Fig. 2, as the lidar signal error is within ± 10%, the error of the 532 nm optical depth solution is only 1.78%. Therefore, the random lidar signal error has a weaker effect on the extinction profile solution by CIA. $f(r_1)$ and $f(r_{1h})$ are the two integrations of the slant and horizontal lidar signals, respectively. According to Eq.6, the effect of error in lidar signals on the optical depth solution by CIA is made through its affecting the ratio of $f(r_1)$ to $f(r_{1h})$. So, If there are similar systematic errors in the horizontal and slant lidar signals, they can be counteracted with a small effect.

Table 3. Optical depth solution error caused by random lidar signal error

D	0.05	0.1	0.2
$\Delta\tau_{a,1}$(%)	0.43	0.85	1.69
$\Delta\tau_{a,2}$(%)	1.12	1.78	4.86

(2) *Effect of error in horizontal optical depth* $\tau_{ah}(r_0, r_{1h})$

The solution by CIA is relative to the optical depth $\tau_{ah}(r_0, r_{1h})$ through its affecting the value G defined in Eq.7. On the ground, the aerosol scattering is usually dominant. Neglecting molecular scattering, it can be derived from Eq.7 that:

$$\frac{\Delta G}{G} = X\frac{\Delta\tau_{ah}(r_0, r_{1h})}{\tau_{ah}(r_0, r_{1h})}, \quad X = \frac{2\tau_{ah}\exp(-2\tau_{ah})}{1-\exp(-2\tau_{ah})} . \tag{18}$$

Here X changes between 0 and 1, and it is a decreasing function of the horizontal optical depth. As the depth is very small, $X \approx 1$. As the depth is equal to 0.6, 1 and 3, $X = 0.517$, 0.313 and 0.0149, respectively. The larger the value X is, the stronger the effect of the depth error on G. Thus, the larger the depth is, the weaker its error effect on the solution by CIA. The range Δr, corresponding to ground-level aerosol optical depth being unity, is about 6.8 km and 1.92 km for the clear and turbid models, respectively. Next, the optical depth is selected as a typical value. In the selection, $r_{1h} - r_0 = 6.8$ km and 1.92 km ($r_{1h} = 7$ km and 2.12

km) for the two models.

Fig. 3 shows the inversion results under the condition of a 10% overestimated error in $\tau_{ah}(r_0, r_{1h})$ for the case of $r_1 = 8$ km and $r_{1h} = 8$ km. An assumption of the homogeneous atmospheric optical property along the horizontal laser path can usually be suitable. And as the extinction coefficient is larger, the optical depth solution derived from lidar signals is usually better. So, an accuracy better than 10% in the horizontal optical depth derived from the ground-level lidar echoes can usually be expected. As shown in Fig. 3, under the 10% error the vertical extinction coefficients retrieved by CIA are overestimated, but all inversion results are satisfactory. The errors in the optical depth solutions are 5.9% and 3.4% for $\lambda = 1060$ nm and 532 nm, respectively. In addition, the smaller r_1 is, the better the solution under the same error of $\tau_{ah}(r_0, r_{1h})$.

(3) *Effect of uncertainty in* k_a

Figures 4–5 show the variation of the far-end extinction coefficient solution, $\sigma_a(r_1)$, with k_a in the two cases of $r_1 = 8$ km and 2 km, respectively, and Figs. 6–7 show the percentage errors of the corresponding optical depth solutions caused by uncertainty in k_a. The true value of k_a is 40. As shown in Figs. 4–5, as far as the 1060 nm wavelength is concerned, there is the weaker effect of error in k_a on solutions $\sigma_a(r_1)$ and $\tau_a(r_0, r_1)$. Especially for the case of $r_1 = 2$ km, as k_a varies between 20 and 60 (its error is within $\pm$ 20), the maximum deviation of $\sigma_a(r_1)$ with its exact value is 12%, and the maximum error in $\tau_a(r_0, r_1)$ is 2.3%. But in the case with the shorter wavelength of $\lambda = 532$ nm, solutions $\sigma_a(r_1)$ and $\tau_a(r_0, r_1)$ are much more sensitive to the variation of k_a, especially for $r_1 = 8$ km. As $r_1 = 8$ km and $k_a > 43.3$ (only with an error larger than 3.3), solution $\sigma_a(r_1)$ is negative. This is why this paper takes $\delta^{(0)} = 0$ in the two-wavelength algorithm presented in last section. As $r_1 = 2$ km, if the error in k_a is less than 10, the optical depth accuracy better than 1.1% and 7.3% can be obtained for $\lambda = 1060$ nm and 532 nm, respectively.

In last simulations, true k_a is height-independent. Next, in the case of height-dependent k_a and aerosol size distribution, the effect of the error in k_a on the solution by CIA is analyzed according to Fig. 8. In Figs. 8–9, there are the urban and continent extinction profiles in the height range of 0–2 km and above 2 km, respectively. In the range of 0–2 km, k_a is equal to 55.9 and 46.6 for $\lambda = 1060$ nm and 532 nm, respectively, and above 2 km $k_a = 37.8$ and 38.1. Here k_a is closely related to height and wavelength. In Fig. 8, $k_a = 55.9$ and 46.6 (urban) for $\lambda = 1060$ nm and 532 nm are selected in simulations. For both the wavelengths, the extinction profile solutions are very good in the height range less than 3 km, but they get worse with the increasing of the height, especially for the range above 5 km. The solution errors in the optical depths between 0.2 km and 8 km are 3.9% and 1.8% for $\lambda = 1060$ nm and 532 nm, respectively, being quite satisfactory.

Among all error factors the uncertainty in k_a usually has the most significant effect on the extinction profile solution. Therefore, a method for the simultaneous retrieval of extinction profile and k_a would be very significant.

c. *Inversion results of joint* $\sigma_a(r), k_a, v^*$ *and* n_i

The inversion results of $\sigma_a(r), k_a, v^*$ and n_i, simultaneously derived from the two-wavelength lidar signals, are shown in Figs. 9–10 and Tables 4–6. Here $\Delta\tau_{a,1}$ and $\Delta\tau_{a,2}$ indicate the percentage errors of the optical depth solutions between r_0 and r_1 for $\lambda = 1060$ and 532 nm, respectively.

Table 4 shows the inversion results without the error in all input parameters except for an assumption of height-independent k_a. For the clear aerosol model with height-independent k_a, quite good solutions are obtained for the two cases of $r_1 = 8$ km and 2 km. The solution of k_a is 38.1, and the true value of k_a for $\lambda = 532$ nm is 38.1. The solution of ν^* is 3.03, and its true value is 3.029. The imaginary part solution of 0.0069 is between the imaginary parts of the fine and coarse aerosol, which seems to be reasonable. The errors in the optical depth solutions are all less than 0.15% for both wavelengths and all r_1. For the turbid aerosol model with height-dependent k_a, the solutions are also good but have the larger error. The solutions of k_a are 45.8 and 43.9 for $r_1 = 8$ km and 2 km, respectively. They are all between 532 nm-wavelength urban k_a (46.6) and its continent k_a (38.1) but close to the urban (lower atmospheric) k_a. The solution of ν^* is about 3.3 for every r_1, being very close to the urban ν^* (3.358). The larger imaginary part solution of about 0.01 is between the imaginary parts of fine soot and coarse aerosol, owing to the larger volume percentage of strong absorbing fine soot in the urban model. The errors in the optical depth solutions are all less than 5.8% for both wavelengths and all r_1. The smaller r_1 is, the better the accuracy of the optical depth solution. In the model k_a is quite different for the wavelengths of 1060 nm and 532 nm. And because k_a retrieved from the 532 nm lidar signals is used in determining the 1060 nm extinction profile, there is the better accuracy in the 532 nm-wavelength solution. Extinction profile solutions only for $r_1 = 8$ km are shown in Figs. 9-10 for the clear and turbid models, respectively. In the case of the clear model, there is almost no error in the solution. In the case of the turbid model, the extinction profile solutions are also satisfactory, but they have the larger error for the heights above 5 km.

Table 4. Inversion results of k_a, τ_a, n_i and ν^* without the error in all input parameters except for an assumption of height-independent k_a

Model	r_1	$k_{a,s}$	ν^*	n_i	$\Delta\tau_{a,1}$(%)	$\Delta\tau_{a,2}$(%)
Clear	8 km	38.1	3.03	0.0069	0.16	0.15
	2 km	38.1	3.03	0.0069	0.04	0.01
Turbid	8 km	45.8	3.30	0.0107	5.8	2.7
	2 km	43.9	3.36	0.0092	0.2	0.1

Table 5. Inversion Results of k_a, τ_a, n_i and ν^* in the case of the error of 10% or -10% in optical depth $\tau_{ah}(r_0, r_{1h})$

Model	r_1	$k_{a,s}$	ν^*	n_i	$\Delta\tau_{a,1}$(%)	$\Delta\tau_{a,2}$(%)
Clear	8 km	38.9 / 37.2	2.98 / 3.10	0.0073 / 0.0072	6.3 / -7.2	2.5 / -2.7
	2 km	38.7 / 37.4	2.97 / 3.09	0.0072 / 0.0063	5.7 / -6.4	1.9 / -2.3
Turbid	8 km	52.9 / 39.4	3.27 / 3.32	0.0158 / 0.0068	14.6 / -4.1	10.4 / -5.5
	2 km	51.8 / 38.5	3.33 / 3.38	0.0151 / 0.0052	9.2 / -9.1	7.3 / -7.7

Table 5 shows inversion results of k_a, τ_a and ν^* in the case of the error of 10% or -10% in horizontal optical depth $\tau_{ah}(r_0, r_{1h})$. The first and second set of digits shown in the five columns of Table 4 correspond to the cases of the errors of 10% and -10%, respectively. For the clear aerosol model, all the solutions of k_a, ν^* and τ_a are very good. The deviation of the solution $k_{a,s}$ to the true 532 nm-wavelength k_a is less than 0.9. The maximum deviation of the solution ν^* to its true value is less than 0.08. The errors of the optical depth solutions are within $\pm$ 7.2% and $\pm$ 2.7% for $\lambda = 1060$ nm and 532 nm, respectively. The smaller r_1 is,

the smaller the error. The imaginary part solution changes between 0.0063 and 0.0073. Compared with the result withont the error in the input parameters, the variation is very small, being less than 0.0007. For the turbid aerosol model, the worse solutions can be obtained, but they seem to be reasonable. The solutions of k_a change between 37.8 and 52.9, and their deviations to the 532 nm-wavelength urban k_a are within ± 9 for every case. The maximum deviation of the solution v^* to the true urban value is less than 0.1. The errors of the optical depth solutions are less than 15% and 11% for $\lambda = 1060$ nm and 532 nm, respectively. The imaginary part solution changes between 0.0052 and 0.0158. The positive error of $\tau_{ah}(r_0, r_{1h})$ can result in a larger imaginary part solution. All the solutions have a deviation less than 0.006 to the imaginary part solution without the error in the input parameters (shown in Table 4). So, it is estimated that the imaginary part error caused by ± 10% error in the horizontal optical depth $\tau_{ah}(r_0, r_{1h})$ is within 0.006.

Table 6. Inversion results of k_a, τ_a, n_i, and v^* in the case of the error of 10% or −10% in far-end lidar signal

Model	r_1	$k_{a,r}$	v^*	n_i	$\Delta\tau_{a,1}$(%)	$\Delta\tau_{a,2}$(%)
Clear	8 km	36.4 / 43.9	3.02 / 3.05	0.0058 / 0.0106	−2.1 / 1.7	−2.7 / 3.2
	2 km	36.3 / 40.2	3.02 / 3.04	0.0058 / 0.0083	−2.2 / 2.1	−2.9 / 3.0
Turbid	8 km	41.2 / 53.3	3.25 / 3.35	0.0077 / 0.0165	3.4 / 8.2	−2.6 / 8.8
	2 km	38.0 / 53.5	3.32 / 3.40	0.0051 / 0.0167	−2.5 / 2.9	−5.0 / 6.2

As analyzed above, there is a weak effect of the random lidar signal errors on the optical depth solution by CIA. Because of the fact, it is found that the random signal error has a weak effect on the solution k_a in the case of no error in the far-end lidar signal. However, the far-end signal error can have a significant effect on the solution of k_a. Table 6 shows the inversion results of k_a, τ_a and v^* in the two cases of 10% and −10% errors in the far-end signal, listed with the first and second set of digits, respectively. For the clear aerosol model, the maximum error of the solution v^* is 0.02, the error in k_a is within ± 5, and the errors of optical depth solutions are within ± 2.2% and ± 3.2% for $\lambda = 1060$ nm and 532 nm, respectively. The variation of the imaginary part solution is less than 0.006. For the turbid aerosol model, the deviation of the solution k_a to the 532 nm-wavelength urban k_a is within ± 10 for every case. The maximum deviation of the solution v^* to the true urban value is only 0.07. The errors of optical depth solutions are less than 9.3% for both $\lambda = 1060$ nm and $\lambda = 532$ nm. The solutions of aerosol size distribution and its optical depth are very good, but the far-end lidar signal error has a significant effect on the solution of k_a. The imaginary part solution changes between 0.0051 and 0.0167. In comparison of the results in Table 6 and Table 4, the imaginary part error caused by the error of ± 10% in the horizontal optical depth $\tau_{ah}(r_0, r_{1h})$ is within 0.007. The mean value of two solutions, corresponding with the 10% and −10% errors in the far-end signal, has a deviation less than 0.002 to the imaginary part solution without the error in the input parameters. So, the mean imaginary part solution of many observations would be much better if the error in the far-end signal is random.

According to Table 2 and Tables 4–6, it is concluded that the retrieved aerosol size distribution, the extinction to backscatter ratio and its imaginary part basically reflect the aerosol characteristic in the lower atmosphere.

Other error factors such as the error in E / E_h are usually less important.

5. Discussion and conclusion

How to determine the far-end boundary value is a key difficulty of the backward integration algorithm to the lidar equation. The present CIA uses the lidar signals and optical depth derived from the signals along the ground-level horizontal path as the constraint information in determining the value along the slant path. One of its advantages is without an assumption of the homogeneous atmosphere near the far-end. Another advantage is that the lidar constant C does not need to be determined for the simultaneous retrieval of aerosol extinction and extinction to backscatter ratio. In some lidar application it does need.

The analytical solution of CIA is obtained. The smaller the vertical (or slant) far-end distance is, the better the extinction profile solution. And because the solution does not depend on the aerosol extinction to backscatter ratio in the case of no molecular scattering and the constant ratio, CIA is especially suitable for the lidar measurements of the aerosol extinction coefficient distribution in the boundary layer.

The main error factors of the solution by CIA are the error of lidar signals, the measurement error of optical depth $\tau_{ah}(r_{0h}, r_{1h})$ along ground-level horizontal path and the uncertainty of k_a especially the last one. The random lidar error can result in a vibrating deviation of the extinction profile solution to its true profile, and they have a weak effect on the optical depth solution. If the error of optical depth $\tau_{ah}(r_{0h}, r_{1h})$ is within 10%, a satisfactory solution by CIA can be obtained. For the case of constant k_a, if its error is within 10, the caused error in the 1060 nm optical depth solution can be less than 3%., but there can be a larger error in the 532 nm solution for a large r_1. The simultaneous retrieval of extinction profile and k_a would be very significant. For the case of height-dependent k_a, to select the lower atmospheric k_a can generally produce a better solution. The shorter the wavelength is, the larger the solution error caused by the uncertainty in k_a. Based on the property, the aerosol extinction profile, the extinction to backscatter ratio, the size distribution and the imaginary part of its reflective index can be simultaneously retrieved from the multi-wavelength lidar signals. In this paper, only two-wavelength inversion algorithm is analyzed, but it can be used in the multi-wavelength case. Under the case, more aerosol information including the non-Junge size distribution can be obtained. The preliminary simulation results are reasonable. A main error factor is dependence of aerosol extinction to backscatter ratio with height and wavelength. In addition, to decrease error in the far-end lidar signal is important for improving the solutions. The mean imaginary part solution of many observations would be much better if the error in the far-end signal is random. The aerosol size distribution, the extinction to backscatter ratio and its imaginary part retrieved mainly reflect the aerosol characteristic in the lower atmosphere.

REFERENCES

Elterman, L., 1964: Parameters for attenuation in the atmospheric windows for fifteen wavelengths. *Appl. Opt.*, **3**, 745-749.

Fernald, F. G., 1984: Analysis of atmospheric lidar observation: some comments. *Appl. Opt.*, **23**, 652-655.

Ferguson J. A., and D. H. Stephens 1983: Algorithm for inverting lidar return. *Appl. Opt.*, **22**, 3673-3675.

Klett, J. D., 1981: Stable analytical inversion solutions for processing lidar returns. *Appl. Opt.*, **20**, 211-220.

Lenoble, J., 1985: Radiative Transfer in Scattering and Absorbing Atmospheres: Standard Computational Procedures. A. Deepak Publislting, Hampton, Va., 121-127.

Potter J. F., 1987: Two-frequency lidar inversion technique. *Appl. Opt.*, **26**, 1250-1256.

Qiu Jinhuan, 1988: Sensitivity of lidar equation solution to boundary values and determination of the values. *Adv. Atmos. Sci.*, **5**, 229–241.

Qiu Jinhuan, 1995: Two-wavelength lidar measurement of cloud-aerosol optical properties. *Adv. Atmos. Sci.*, **12**, 176–177.

Sasano Y., and H. Nakene, 1984: Significance of the extinction / backscatter ratio and the boundary value term in the solution for the two-component lidar equation. *Appl. Opt.*, **23**, 11–13.

Spinhirne, J. D., J. A. Reagan, and B. M. Herman, 1980: Vertical distribution of aerosol extinction cross section and inference of aerosol imaginary index in the troposphere by lidar technique. *J. Appl. Meteor.*, **19**, 426–438.